

SegFormer: Simple and Efficient Design for Semantic Segmentation with Transformers

Enze Xie¹, Wenhui Wang², Zhiding Yu³, Anima Anandkumar^{3,4}, Jose M. Alvarez³, Ping Luo¹

¹The University of Hong Kong ²Nanjing University ³NVIDIA ⁴Caltech

Abstract

We present SegFormer, a simple, efficient yet powerful semantic segmentation framework which unifies Transformers with lightweight multilayer perceptron (MLP) decoders. SegFormer has two appealing features: 1) SegFormer comprises a novel hierarchically structured Transformer encoder which outputs multiscale features. It does not need positional encoding, thereby avoiding the interpolation of positional codes which leads to decreased performance when the testing resolution differs from training. 2) SegFormer avoids complex decoders. The proposed MLP decoder aggregates information from different layers, and thus combining both local attention and global attention to render powerful representations. We show that this simple and lightweight design is the key to efficient segmentation on Transformers. We scale our approach up to obtain a series of models from SegFormer-B0 to SegFormer-B5, reaching significantly better performance and efficiency than previous counterparts. For example, SegFormer-B4 achieves 50.3% mIoU on ADE20K with 64M parameters, being 5× smaller and 2.2% better than the previous best method. Our best model, SegFormer-B5, achieves 84.0% mIoU on Cityscapes validation set and shows excellent zero-shot robustness on Cityscapes-C. Code will be released at: github.com/NVlabs/SegFormer.

1 Introduction

Semantic segmentation is a fundamental task in computer vision and enables many downstream applications. It is related to image classification since it produces per-pixel category prediction instead of image-level prediction. This relationship is pointed out and systematically studied in a seminal work [1], where the authors used fully convolutional networks (FCNs) for semantic segmentation tasks. Since then, FCN has inspired many follow-up works and has become a predominant design choice for dense prediction.

Since there is a strong relation between classification and semantic segmentation, many state-of-the-art semantic segmentation frameworks are variants of popular architectures for image classification on ImageNet. Therefore, designing backbone architectures has remained an active area in semantic segmentation. Indeed, starting from early methods using VGGs [1, 2], to the latest methods with significantly deeper and more powerful backbones [3], the evolution of backbones has dramatically pushed the performance boundary of

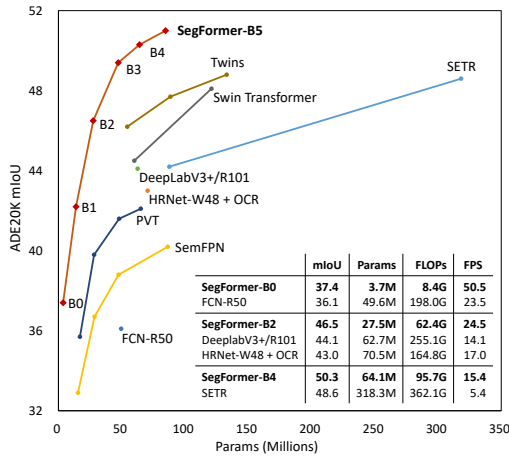


Figure 1: Performance vs. model efficiency on ADE20K. All results are reported with single model and single-scale inference. SegFormer achieves a new state-of-the-art 51.0% mIoU while being significantly more efficient than previous methods.

semantic segmentation. Besides backbone architectures, another line of work formulates semantic segmentation as a structured prediction problem, and focuses on designing modules and operators, which can effectively capture contextual information. A representative example in this area is dilated convolution [4, 5], which increases the receptive field by “inflating” the kernel with holes.

Witnessing the great success in natural language processing (NLP), there has been a recent surge of interest to introduce Transformers to vision tasks. Dosovitskiy et al. [6] proposed vision Transformer (ViT) for image classification. Following the Transformer design in NLP, the authors split an image into multiple linearly embedded patches and feed them into a standard Transformer with positional embeddings (PE), leading to an impressive performance on ImageNet. In semantic segmentation, Zheng et al. [7] proposed SETR to demonstrate the feasibility of using Transformers in this task.

SETR adopts ViT as a backbone and incorporates several CNN decoders to enlarge feature resolution. Despite the good performance, ViT has some limitations: 1) ViT outputs single-scale low-resolution features instead of multi-scale ones. 2) It has high computation cost on large images. To address these limitations, Wang et al. [8] proposed a pyramid vision Transformer (PVT), a natural extension of ViT with pyramid structures for dense prediction. PVT shows considerable improvements over the ResNet counterpart on object detection and semantic segmentation. However, together with other emerging methods such as Swin Transformer [9] and Twins [10], these methods mainly consider the design of the Transformer encoder, neglecting the contribution of the decoder for further improvements.

This paper introduces SegFormer, a cutting-edge Transformer framework for semantic segmentation that jointly considers efficiency, accuracy, and robustness. In contrast to previous methods, our framework redesigns both the encoder and the decoder. The key novelties of our approach are:

- A novel positional-encoding-free and hierarchical Transformer encoder.
- A lightweight All-MLP decoder design that yields a powerful representation without complex and computationally demanding modules.
- As shown in Figure 1, SegFormer sets new a state-of-the-art in terms of efficiency, accuracy and robustness in three publicly available semantic segmentation datasets.

First, the proposed encoder avoids interpolating positional codes when performing inference on images with resolutions different from the training one. As a result, our encoder can easily adapt to arbitrary test resolutions without impacting the performance. In addition, the hierarchical part enables the encoder to generate both high-resolution fine features and low-resolution coarse features, this is in contrast to ViT that can only produce single low-resolution feature maps with fixed resolutions. Second, we propose a lightweight MLP decoder where the key idea is to take advantage of the Transformer-induced features where the attentions of lower layers tend to stay local, whereas the ones of the highest layers are highly non-local. By aggregating the information from different layers, the MLP decoder combines both local and global attention. As a result, we obtain a simple and straightforward decoder that renders powerful representations.

We demonstrate the advantages of SegFormer in terms of model size, run-time, and accuracy on three publicly available datasets: ADE20K, Cityscapes, and COCO-Stuff. On Cityscapes, our lightweight model, SegFormer-B0, without accelerated implementations such as TensorRT, yields 71.9% mIoU at 48 FPS, which, compared to ICNet [11], represents a relative improvement of 60% and 4.2% in latency and performance, respectively. Our largest model, SegFormer-B5, yields 84.0% mIoU, which represents a relative 1.8% mIoU improvement while being $5 \times$ faster than SETR [7]. On ADE20K, this model sets a new state-of-the-art of 51.8% mIoU while being $4 \times$ smaller than SETR. Moreover, our approach is significantly more robust to common corruptions and perturbations than existing methods, therefore being suitable for safety-critical applications. Code will be publicly available.

2 Related Work

Semantic Segmentation. Semantic segmentation can be seen as an extension of image classification from image level to pixel level. In the deep learning era [12–16], FCN [1] is the fundamental work of semantic segmentation, which is a fully convolution network that performs pixel-to-pixel classification in an end-to-end manner. After that, researchers focused on improving FCN from different aspects such as: enlarging the receptive field [17–19, 5, 2, 4, 20]; refining the contextual information [21–

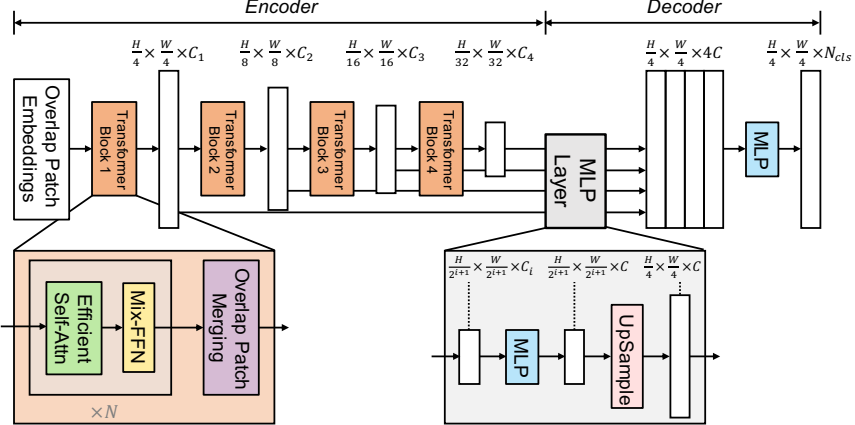


Figure 2: **The proposed SegFormer framework** consists of two main modules: A hierarchical Transformer encoder to extract coarse and fine features; and a lightweight All-MLP decoder to directly fuse these multi-level features and predict the semantic segmentation mask. “FFN” indicates feed-forward network.

29]; introducing boundary information [30–37]; designing various attention modules [38–46]; or using AutoML technologies [47–51]. These methods significantly improve semantic segmentation performance at the expense of introducing many empirical modules, making the resulting framework computationally demanding and complicated. More recent methods have proved the effectiveness of Transformer-based architectures for semantic segmentation [7, 46]. However, these methods are still computationally demanding.

Transformer backbones. ViT [6] is the first work to prove that a pure Transformer can achieve state-of-the-art performance in image classification. ViT treats each image as a sequence of tokens and then feeds them to multiple Transformer layers to make the classification. Subsequently, DeiT [52] further explores a data-efficient training strategy and a distillation approach for ViT. More recent methods such as T2T ViT [53], CPVT [54], TNT [55], CrossViT [56] and LocalViT [57] introduce tailored changes to ViT to further improve image classification performance.

Beyond classification, PVT [8] is the first work to introduce a pyramid structure in Transformer, demonstrating the potential of a pure Transformer backbone compared to CNN counterparts in dense prediction tasks. After that, methods such as Swin [9], CvT [58], CoaT [59], LeViT [60] and Twins [10] enhance the local continuity of features and remove fixed size position embedding to improve the performance of Transformers in dense prediction tasks.

Transformers for specific tasks. DETR [52] is the first work using Transformers to build an end-to-end object detection framework without non-maximum suppression (NMS). Other works have also used Transformers in a variety of tasks such as tracking [61, 62], super-resolution [63], ReID [64], Colorization [65], Retrieval [66] and multi-modal learning [67, 68]. For semantic segmentation, SETR [7] adopts ViT [6] as a backbone to extract features, achieving impressive performance. However, these Transformer-based methods have very low efficiency and, thus, difficult to deploy in real-time applications.

3 Method

This section introduces SegFormer, our efficient, robust, and powerful segmentation framework without hand-crafted and computationally demanding modules. As depicted in Figure 2, SegFormer consists of two main modules: (1) a hierarchical Transformer encoder to generate high-resolution coarse features and low-resolution fine features; and (2) a lightweight All-MLP decoder to fuse these multi-level features to produce the final semantic segmentation mask.

Given an image of size $H \times W \times 3$, we first divide it into patches of size 4×4 . Contrary to ViT that uses patches of size 16×16 , using smaller patches favors the dense prediction task. We then use these patches as input to the hierarchical Transformer encoder to obtain multi-level features at $\{1/4, 1/8, 1/16, 1/32\}$ of the original image resolution. We then pass these multi-level features to the All-MLP decoder to predict the segmentation mask at a $\frac{H}{4} \times \frac{W}{4} \times N_{cls}$ resolution, where N_{cls} is the

number of categories. In the rest of this section, we detail the proposed encoder and decoder designs and summarize the main differences between our approach and SETR.

3.1 Hierarchical Transformer Encoder

We design a series of Mix Transformer encoders (MiT), MiT-B0 to MiT-B5, with the same architecture but different sizes. MiT-B0 is our lightweight model for fast inference, while MiT-B5 is the largest model for the best performance. Our design for MiT is partly inspired by ViT but tailored and optimized for semantic segmentation.

Hierarchical Feature Representation. Unlike ViT that can only generate a single-resolution feature map, the goal of this module is, given an input image, to generate CNN-like multi-level features. These features provide high-resolution coarse features and low-resolution fine-grained features that usually boost the performance of semantic segmentation. More precisely, given an input image with a resolution of $H \times W \times 3$, we perform patch merging to obtain a hierarchical feature map F_i with a resolution of $\frac{H}{2^{i+1}} \times \frac{W}{2^{i+1}} \times C_i$, where $i \in \{1, 2, 3, 4\}$, and C_{i+1} is larger than C_i .

Overlapped Patch Merging. Given an image patch, the patch merging process used in ViT, unifies a $N \times N \times 3$ patch into a $1 \times 1 \times C$ vector. This can easily be extended to unify a $2 \times 2 \times C_i$ feature path into a $1 \times 1 \times C_{i+1}$ vector to obtain hierarchical feature maps. Using this, we can shrink our hierarchical features from $F_1 (\frac{H}{4} \times \frac{W}{4} \times C_1)$ to $F_2 (\frac{H}{8} \times \frac{W}{8} \times C_2)$, and then iterate for any other feature map in the hierarchy. This process was initially designed to combine non-overlapping image or feature patches. Therefore, it fails to preserve the local continuity around those patches. Instead, we use an overlapping patch merging process. To this end, we define K , S , and P , where K is the patch size, S is the stride between two adjacent patches, and P is the padding size. In our experiments, we set $K = 7$, $S = 4$, $P = 3$, and $K = 3$, $S = 2$, $P = 1$ to perform overlapping patch merging to produce features with the same size as the non-overlapping process.

Efficient Self-Attention. The main computation bottleneck of the encoders is the self-attention layer. In the original multi-head self-attention process, each of the heads Q , K , V have the same dimensions $N \times C$, where $N = H \times W$ is the length of the sequence, the self-attention is estimated as:

$$\text{Attention}(Q, K, V) = \text{Softmax}\left(\frac{QK^T}{\sqrt{d_{\text{head}}}}\right)V. \quad (1)$$

The computational complexity of this process is $O(N^2)$, which is prohibitive for large image resolutions. Instead, we use the sequence reduction process introduced in [8]. This process uses a reduction ratio R to reduce the length of the sequence as follows:

$$\begin{aligned} \hat{K} &= \text{Reshape}\left(\frac{N}{R}, C \cdot R\right)(K) \\ K &= \text{Linear}(C \cdot R, C)(\hat{K}), \end{aligned} \quad (2)$$

where K is the sequence to be reduced, $\text{Reshape}\left(\frac{N}{R}, C \cdot R\right)(K)$ refers to reshape K to the one with shape of $\frac{N}{R} \times (C \cdot R)$, and $\text{Linear}(C_{in}, C_{out})(\cdot)$ refers to a linear layer taking a C_{in} -dimensional tensor as input and generating a C_{out} -dimensional tensor as output. Therefore, the new K has dimensions $\frac{N}{R} \times C$. As a result, the complexity of the self-attention mechanism is reduced from $O(N^2)$ to $O(\frac{N^2}{R})$. In our experiments, we set R to [64, 16, 4, 1] from stage-1 to stage-4.

Mix-FFN. ViT uses positional encoding (PE) to introduce the location information. However, the resolution of PE is fixed. Therefore, when the test resolution is different from the training one, the positional code needs to be interpolated and this often leads to dropped accuracy. To alleviate this problem, CPVT [54] uses 3×3 Conv together with the PE to implement a data-driven PE. We argue that positional encoding is actually not necessary for semantic segmentation. Instead, we introduce Mix-FFN which considers the effect of zero padding to leak location information [69], by directly using a 3×3 Conv in the feed-forward network (FFN). Mix-FFN can be formulated as:

$$\mathbf{x}_{out} = \text{MLP}(\text{GELU}(\text{Conv}_{3 \times 3}(\text{MLP}(\mathbf{x}_{in})))) + \mathbf{x}_{in}, \quad (3)$$

where \mathbf{x}_{in} is the feature from the self-attention module. Mix-FFN mixes a 3×3 convolution and an MLP into each FFN. In our experiments, we will show that a 3×3 convolution is sufficient to provide positional information for Transformers. In particular, we use depth-wise convolutions for reducing the number of parameters and improving efficiency.

3.2 Lightweight All-MLP Decoder

SegFormer incorporates a lightweight decoder consisting only of MLP layers and this avoiding the hand-crafted and computationally demanding components typically used in other methods. The key to enabling such a simple decoder is that our hierarchical Transformer encoder has a larger effective receptive field (ERF) than traditional CNN encoders.

The proposed All-MLP decoder consists of four main steps. First, multi-level features F_i from the MiT encoder go through an MLP layer to unify the channel dimension. Then, in a second step, features are up-sampled to 1/4th and concatenated together. Third, a MLP layer is adopted to fuse the concatenated features F . Finally, another MLP layer takes the fused feature to predict the segmentation mask M with a $\frac{H}{4} \times \frac{W}{4} \times N_{cls}$ resolution, where N_{cls} is the number of categories. This lets us formulate the decoder as:

$$\begin{aligned}\hat{F}_i &= \text{Linear}(C_i, C)(F_i), \forall i \\ \hat{F}_i &= \text{Upsample}\left(\frac{W}{4} \times \frac{W}{4}\right)(\hat{F}_i), \forall i \\ F &= \text{Linear}(4C, C)(\text{Concat}(\hat{F}_i)), \forall i \\ M &= \text{Linear}(C, N_{cls})(F),\end{aligned}\tag{4}$$

where M refers to the predicted mask, and $\text{Linear}(C_{in}, C_{out})(\cdot)$ refers to a linear layer with C_{in} and C_{out} as input and output vector dimensions respectively.

Effective Receptive Field Analysis.

For semantic segmentation, maintaining large receptive field to include context information has been a central issue [5, 19, 20]. Here, we use effective receptive field (ERF) [70] as a toolkit to visualize and interpret why our MLP decoder design is so effective on Transformers. In Figure 3, we visualize ERFs of the four encoder stages and the decoder heads for both DeepLabv3+ and SegFormer. We can make the following observations:

- The ERF of DeepLabv3+ is relatively small even at Stage-4, the deepest stage.
- SegFormer’s encoder naturally produces local attentions which resemble convolutions at lower stages, while able to output highly non-local attentions that effectively capture contexts at Stage-4.
- As shown with the zoom-in patches in Figure 3, the ERF of the MLP head (blue box) differs from Stage-4 (red box) with a significant stronger local attention besides the non-local attention.

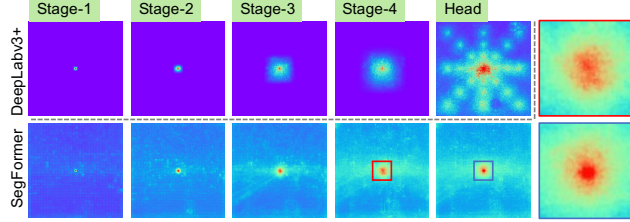


Figure 3: **Effective Receptive Field (ERF) on Cityscapes** (average over 100 images). Top row: DeepLabv3+. Bottom row: SegFormer. ERFs of the four stages and the decoder heads of both architectures are visualized. Best viewed with zoom in.

The limited receptive field in CNN requires one to resort to context modules such as ASPP [18] that enlarge the receptive field but inevitably become heavy. Our decoder design benefits from the non-local attention in Transformers and leads to a larger receptive field without being complex. The same decoder design, however, does not work well on CNN backbones since the overall receptive field is upper bounded by the limited one at Stage-4, and we will verify this later in Table 1d,

More importantly, our decoder design essentially takes advantage of a Transformer induced feature that produces both highly local and non-local attention at the same time. By unifying them, our MLP decoder renders complementary and powerful representations by adding few parameters. This is another key reason that motivated our design. Taking the non-local attention from Stage-4 alone is not enough to produce good results, as will be verified in Table 1d.

3.3 Relationship to SETR.

SegFormer contains multiple more efficient and powerful designs compared with SETR [7]:

- We only use ImageNet-1K for pre-training. ViT in SETR is pre-trained on larger ImageNet-22K.

- SegFormer’s encoder has a hierarchical architecture, which is smaller than ViT and can capture both high-resolution coarse and low-resolution fine features. In contrast, SETR’s ViT encoder can only generate single low-resolution feature map.
- We remove Positional Embedding in encoder, while SETR uses fixed shape Positional Embedding which decreases the accuracy when the resolution at inference differs from the training ones.
- Our MLP decoder is more compact and less computationally demanding than the one in SETR. This leads to a *negligible* computational overhead. In contrast, SETR requires heavy decoders with multiple 3×3 convolutions.

4 Experiments

4.1 Experimental Settings

Datasets: We used three publicly available datasets: Cityscapes [71], ADE20K [72] and COCO-Stuff [73]. ADE20K is a scene parsing dataset covering 150 fine-grained semantic concepts consisting of 20210 images. Cityscapes is a driving dataset for semantic segmentation consisting of 5000 fine-annotated high resolution images with 19 categories. COCO-Stuff covers 172 labels and consists of 164k images: 118k for training, 5k for validation, 20k for test-dev and 20k for the test-challenge.

Implementation details: We used the *mmsegmentation*¹ codebase and train on a server with 8 Tesla V100. We pre-train the encoder on the Imagenet-1K dataset and randomly initialize the decoder. During training, we applied data augmentation through random resize with ratio 0.5-2.0, random horizontal flipping, and random cropping to 512×512 , 1024×1024 , 512×512 for ADE20K, Cityscapes and COCO-Stuff, respectively. Following [9] we set crop size to 640×640 on ADE20K for our largest model B5. We trained the models using AdamW optimizer for 160K iterations on ADE20K, Cityscapes, and 80K iterations on COCO-Stuff. Exceptionally, for the ablation studies, we trained the models for 40K iterations. We used a batch size of 16 for ADE20K and COCO-Stuff, and a batch size of 8 for Cityscapes. The learning rate was set to an initial value of 0.00006 and then used a “poly” LR schedule with factor 1.0 by default. For simplicity, we *did not* adopt widely-used tricks such as OHEM, auxiliary losses or class balance loss. During evaluation, we rescale the short side of the image to training cropping size and keep the aspect ratio for ADE20K and COCO-Stuff. For Cityscapes, we do inference using sliding window test by cropping 1024×1024 windows. We report semantic segmentation performance using mean Intersection over Union (mIoU).

4.2 Ablation Studies

Influence of the size of model. We first analyze the effect of increasing the size of the encoder on the performance and model efficiency. Figure 1 shows the performance vs. model efficiency for ADE20K as a function of the encoder size and, Table 1a summarizes the results for the three datasets. The first thing to observe here is the size of the decoder compared to the encoder. As shown, for the lightweight model, the decoder has only 0.4M parameters. For MiT-B5 encoder, the decoder only takes up to 4% of the total number of parameters in the model. In terms of performance, we can observe that, overall, increasing the size of the encoder yields consistent improvements on all the datasets. Our lightweight model, SegFormer-B0, is compact and efficient while maintaining a competitive performance, showing that our method is very convenient for real-time applications. On the other hand, our SegFormer-B5, the largest model, achieves state-of-the-art results on all three datasets, showing the potential of our Transformer encoder.

Influence of C , the MLP decoder channel dimension. We now analyze the influence of the channel dimension C in the MLP decoder, see Section 3.2. In Table 1b we show performance, flops, and parameters as a function of this dimension. We can observe that setting $C = 256$ provides a very competitive performance and computational cost. The performance increases as C increases; however, it leads to larger and less efficient models. Interestingly, this performance plateaus for channel dimensions wider than 768. Given these results, we choose $C = 256$ for our real-time models SegFormer-B0, B1 and $C = 768$ for the rest.

¹<https://github.com/open-mmlab/mmsegmentation>

Table 1: Ablation studies related to model size, encoder and decoder design.

(a) Accuracy, parameters and flops as a function of the model size on the three datasets. “SS” and “MS” means single/multi-scale test.

| Encoder Model Size | Params | | ADE20K | | Cityscapes | | COCO-Stuff | |
|-----------------------|---------|---------|---------|---------------|------------|---------------|------------|------------|
| | Encoder | Decoder | Flops ↓ | mIoU(SS/MS) ↑ | Flops ↓ | mIoU(SS/MS) ↑ | Flops ↓ | mIoU(SS) ↑ |
| MiT-B0 | 3.4 | 0.4 | 8.4 | 37.4 / 38.0 | 125.5 | 76.2 / 78.1 | 8.4 | 35.6 |
| MiT-B1 | 13.1 | 0.6 | 15.9 | 42.2 / 43.1 | 243.7 | 78.5 / 80.0 | 15.9 | 40.2 |
| MiT-B2 | 24.2 | 3.3 | 62.4 | 46.5 / 47.5 | 717.1 | 81.0 / 82.2 | 62.4 | 44.6 |
| MiT-B3 | 44.0 | 3.3 | 79.0 | 49.4 / 50.0 | 962.9 | 81.7 / 83.3 | 79.0 | 45.5 |
| MiT-B4 | 60.8 | 3.3 | 95.7 | 50.3 / 51.1 | 1240.6 | 82.3 / 83.9 | 95.7 | 46.5 |
| MiT-B5 | 81.4 | 3.3 | 183.3 | 51.0 / 51.8 | 1460.4 | 82.4 / 84.0 | 111.6 | 46.7 |

(b) Accuracy as a function of the MLP dimension C in the decoder on ADE20K.

(c) Mix-FFN vs. positional encoding (PE) for different test resolution on Cityscapes.

(d) Accuracy on ADE20K of CNN and Transformer encoder with MLP decoder. “S4” means stage-4 feature.

| C | Flops ↓ | Params ↓ | mIoU ↑ |
|------|---------|----------|--------|
| 256 | 25.7 | 24.7 | 44.9 |
| 512 | 39.8 | 25.8 | 45.0 |
| 768 | 62.4 | 27.5 | 45.4 |
| 1024 | 93.6 | 29.6 | 45.2 |
| 2048 | 304.4 | 43.4 | 45.6 |

| Inf Res | Enc Type | mIoU ↑ |
|-----------|----------|--------|
| 768×768 | PE | 77.3 |
| 1024×2048 | PE | 74.0 |
| 768×768 | Mix-FFN | 80.5 |
| 1024×2048 | Mix-FFN | 79.8 |

| Encoder | Flops ↓ | Params ↓ | mIoU ↑ |
|----------------------|-------------|-------------|-------------|
| ResNet50 (S1-4) | 69.2 | 29.0 | 34.7 |
| ResNet101 (S1-4) | 88.7 | 47.9 | 38.7 |
| ResNeXt101 (S1-4) | 127.5 | 86.8 | 39.8 |
| MiT-B2 (S4) | 22.3 | 24.7 | 43.1 |
| MiT-B2 (S1-4) | 62.4 | 27.7 | 45.4 |
| MiT-B3 (S1-4) | 79.0 | 47.3 | 48.6 |

Table 2: Comparison to state of the art methods on ADE20K and Cityscapes. SegFormer has significant advantages on #Params, #Flops, #Speed and #Accuracy. Note that for SegFormer-B0 we scale the short side of image to {1024, 768, 640, 512} to get speed-accuracy tradeoffs.

| | Method | Encoder | Params ↓ | ADE20K | | | Cityscapes | | |
|-------------------------|-------------------------|-----------------|-------------|-------------|-------------|-------------|--------------|------------|-------------|
| | | | | Flops ↓ | FPS ↑ | mIoU ↑ | Flops ↓ | FPS ↑ | mIoU ↑ |
| Real-Time | FCN [1] | MobileNetV2 | 9.8 | 39.6 | 64.4 | 19.7 | 317.1 | 14.2 | 61.5 |
| | ICNet [11] | - | - | - | - | - | - | 30.3 | 67.7 |
| | PSPNet [17] | MobileNetV2 | 13.7 | 52.9 | 57.7 | 29.6 | 423.4 | 11.2 | 70.2 |
| | DeepLabV3+ [20] | MobileNetV2 | 15.4 | 69.4 | 43.1 | 34.0 | 555.4 | 8.4 | 75.2 |
| SegFormer (Ours) | MiT-B0 | | 3.8 | 8.4 | 50.5 | 37.4 | 125.5 | 15.2 | 76.2 |
| | | | | - | - | - | 51.7 | 26.3 | 75.3 |
| Non Real-Time | FCN [1] | ResNet-101 | 68.6 | 275.7 | 14.8 | 41.4 | 2203.3 | 1.2 | 76.6 |
| | EncNet [24] | ResNet-101 | 55.1 | 218.8 | 14.9 | 44.7 | 1748.0 | 1.3 | 76.9 |
| | PSPNet [17] | ResNet-101 | 68.1 | 256.4 | 15.3 | 44.4 | 2048.9 | 1.2 | 78.5 |
| | CCNet [41] | ResNet-101 | 68.9 | 278.4 | 14.1 | 45.2 | 2224.8 | 1.0 | 80.2 |
| | DeepLabV3+ [20] | ResNet-101 | 62.7 | 255.1 | 14.1 | 44.1 | 2032.3 | 1.2 | 80.9 |
| | OCRNet [23] | HRNet-W48 | 70.5 | 164.8 | 17.0 | 45.6 | 1296.8 | 4.2 | 81.1 |
| | GSCNN [35] | WideResNet38 | - | - | - | - | - | - | 80.8 |
| | Axial-DeepLab [74] | AxialResNet-XL | - | - | - | - | 2446.8 | - | 81.1 |
| | Dynamic Routing [75] | Dynamic-L33-PSP | - | - | - | - | 270.0 | - | 80.7 |
| | Auto-DeepLab [50] | NAS-F48-ASPP | - | - | - | 44.0 | 695.0 | - | 80.3 |
| | SETR [7] | ViT-Large | 318.3 | - | 5.4 | 50.2 | - | 0.5 | 82.2 |
| | SegFormer (Ours) | MiT-B4 | 64.1 | 95.7 | 15.4 | 51.1 | 1240.6 | 3.0 | 83.8 |
| | SegFormer (Ours) | MiT-B5 | 84.7 | 183.3 | 9.8 | 51.8 | 1447.6 | 2.5 | 84.0 |

Mix-FFN vs. Positional Encoder (PE). In this experiment, we analyze the effect of removing the positional encoding in the Transformer encoder in favor of using the proposed Mix-FFN. To this end, we train Transformer encoders with a positional encoding (PE) and the proposed Mix-FFN and perform inference on Cityscapes with two different image resolutions: 768×768 using a sliding window, and 1024×2048 using the whole image.

Table 1c shows the results for this experiment. As shown, for a given resolution, our approach using Mix-FFN clearly outperforms using a positional encoding. Moreover, our approach is less sensitive to differences in the test resolution: the accuracy drops 3.3% when using a positional encoding with a lower resolution. In contrast, when we use the proposed Mix-FFN the performance drop is reduced to only 0.7%. From these results, we can conclude using the proposed Mix-FFN produces better and more robust encoders than those using positional encoding.

Effective receptive field evaluation. In Section 3.2, we argued that our MLP decoder benefits from Transformers having a larger effective receptive field compared to other CNN models. To quantify this effect, in this experiment, we compare the performance of our MLP-decoder when used with CNN-based encoders such as ResNet or ResNeXt. As shown in Table 1d, coupling our

MLP-decoder with a CNN-based encoder yields a significantly lower accuracy compared to coupling it with the proposed Transformer encoder. Intuitively, as a CNN has a smaller receptive field than the Transformer (see the analysis in Section 3.2), the MLP-decoder is not enough for global reasoning. In contrast, coupling our Transformer encoder with the MLP decoder leads to the best performance. Moreover, for Transformer encoder, it is necessary to combine low-level local features and high-level non-local features instead of only high-level feature.

4.3 Comparison to state of the art methods

We now compare our results with existing approaches on the ADE20K [72], Cityscapes [71] and COCO-Stuff [73] datasets.

ADE20K and Cityscapes: Table 2 summarizes our results including parameters, FLOPS, latency, and accuracy for ADE20K and Cityscapes. In the top part of the table, we report real-time approaches where we include state-of-the-art methods and our results using the MiT-B0 lightweight encoder. In the bottom part, we focus on performance and report the results of our approach and related works using stronger encoders.

As shown, on ADE20K, SegFormer-B0 yields 37.4% mIoU using only 3.8M parameters and 8.4G FLOPs, outperforming all other real-time counterparts in terms of parameters, flops, and latency. For instance, compared to DeeplabV3+ (MobileNetV2), SegFormer-B0 is 7.4 FPS, which is faster and keeps 3.4% better mIoU. Moreover, SegFormer-B5 outperforms all other approaches, including the previous best SETR, and establishes a new state-of-the-art of 51.8%, which is 1.6% mIoU better than SETR while being significantly more efficient.

As also shown in Table 2, our results also hold on Cityscapes. SegFormer-B0 yields 15.2 FPS and 76.2% mIoU (the shorter side of input image being 1024), which represents a 1.3% mIoU improvement and a $2\times$ speedup compared to DeeplabV3+. Moreover, with the shorter side of input image being 512, SegFormer-B0 runs at 47.6 FPS and yields 71.9% mIoU, which is 17.3 FPS faster and 4.2% better than ICNet. SegFormer-B5 archives the best IoU of 84.0%, outperforming all existing methods by at least 1.8% mIoU, and it runs $5\times$ faster and $4\times$ smaller than SETR [7].

On Cityscapes test set, we follow the common setting [20] and merge the validation images to the train set and report results using Imagenet-1K pre-training and also using Mapillary Vistas [76]. As reported in Table 3, using only Cityscapes fine data and Imagenet-1K pre-training, our method achieves 82.2% mIoU outperforming all other methods including SETR, which uses ImageNet-22K pre-training and the additional Cityscapes coarse data. Using Mapillary pre-training, our sets a new state-of-the-art result of 83.1% mIoU. Figure 4 shows qualitative results on Cityscapes, where SegFormer provides better details than SETR and smoother predictions than DeeplabV3+.

COCO-Stuff. Finally, we evaluate SegFormer on the full COCO-Stuff dataset. For comparison, as existing methods do not provide results on this dataset, we reproduce the most representative methods such as DeeplabV3+, OCRNet, and SETR. In this case, the flops on this dataset are the same as those reported for ADE20K. As shown in Table 4, SegFormer-B5 reaches 46.7% mIoU with only 84.7M parameters, which is 0.9% better and $4\times$ smaller than SETR. In summary, these results demonstrate the superiority of SegFormer in semantic segmentation in terms of accuracy, computation cost, and model size.

4.4 Robustness to natural corruptions

Model robustness is important for many safety-critical tasks such as autonomous driving [77]. In this experiment, we evaluate the robustness of SegFormer to common corruptions and perturbations. To

Table 3: Comparison to state of the art methods on Cityscapes test set. IM-1K, IM-22K, Coarse and MV refer to the ImageNet-1K, ImageNet-22K, Cityscapes coarse set and Mapillary Vistas. SegFormer outperforms the compared methods with equal or less extra data.

| Method | Encoder | Extra Data | mIoU |
|--------------------|----------------|----------------|-------------|
| PSPNet [17] | ResNet-101 | IM-1K | 78.4 |
| PSANet [43] | ResNet-101 | IM-1K | 80.1 |
| CCNet [41] | ResNet-101 | IM-1K | 81.9 |
| OCNet [21] | ResNet-101 | IM-1K | 80.1 |
| Axial-DeepLab [74] | AxialResNet-XL | IM-1K | 79.9 |
| SETR [7] | ViT | IM-22K | 81.0 |
| SETR [7] | ViT | IM-22K, Coarse | 81.6 |
| SegFormer | MiT-B5 | IM-1K | 82.2 |
| SegFormer | MiT-B5 | IM-1K, MV | 83.1 |

Table 4: Results on COCO-Stuff full dataset containing all 164K images from COCO 2017 and covers 172 classes.

| Method | Encoder | Params | mIoU |
|-----------------|-----------|-------------|-------------|
| DeeplabV3+ [20] | ResNet50 | 43.7 | 38.4 |
| OCRNet [23] | HRNet-W48 | 70.5 | 42.3 |
| SETR [7] | ViT | 305.7 | 45.8 |
| SegFormer | MiT-B5 | 84.7 | 46.7 |

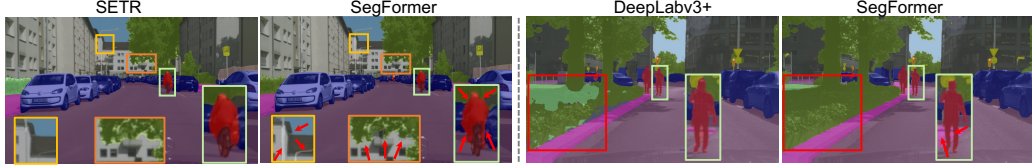


Figure 4: **Qualitative results on Cityscapes.** Compared to SETR, our SegFormer predicts masks with substantially finer details near object boundaries. Compared to DeepLabv3+, SegFormer reduces long-range errors as highlighted in red. Best viewed in screen.

this end, we follow [77] and generate Cityscapes-C, which expands the Cityscapes validation set with 16 types of algorithmically generated corruptions from noise, blur, weather and digital categories. We compare our method to variants of DeepLabV3+ and other methods as reported in [77]. The results for this experiment are summarized in Table 5.

Our method significantly outperforms previous methods, yielding a relative improvement of up to 588% on Gaussian Noise and up to 295% on snow weather. The results indicate the strong robustness of SegFormer, which we envision to benefit safety-critical applications where robustness is important.

Table 5: **Main results on Cityscapes-C.** “DLv3+”, “MBv2”, “R” and “X” refer to DeepLabv3+, MobileNetv2, ResNet and Xception. The mIoUs of compared methods are reported from [77].

| Method | Clean | Blur | | | | Noise | | | | Digital | | | | Weather | | | |
|--------------|-------------|-------------|-------------|-------------|-------------|-------------|-------------|-------------|-------------|-------------|-------------|-------------|-------------|-------------|-------------|-------------|-------------|
| | | Motion | Defoc | Glass | Gauss | Gauss | Impul | Shot | Speck | Bright | Contr | Satur | JPEG | Snow | Spatt | Fog | Frost |
| DLv3+ (MBv2) | 72.0 | 53.5 | 49.0 | 45.3 | 49.1 | 6.4 | 7.0 | 6.6 | 16.6 | 51.7 | 46.7 | 32.4 | 27.2 | 13.7 | 38.9 | 47.4 | 17.3 |
| DLv3+ (R50) | 76.6 | 58.5 | 56.6 | 47.2 | 57.7 | 6.5 | 7.2 | 10.0 | 31.1 | 58.2 | 54.7 | 41.3 | 27.4 | 12.0 | 42.0 | 55.9 | 22.8 |
| DLv3+ (R101) | 77.1 | 59.1 | 56.3 | 47.7 | 57.3 | 13.2 | 13.9 | 16.3 | 36.9 | 59.2 | 54.5 | 41.5 | 37.4 | 11.9 | 47.8 | 55.1 | 22.7 |
| DLv3+ (X41) | 77.8 | 61.6 | 54.9 | 51.0 | 54.7 | 17.0 | 17.3 | 21.6 | 43.7 | 63.6 | 56.9 | 51.7 | 38.5 | 18.2 | 46.6 | 57.6 | 20.6 |
| DLv3+ (X65) | 78.4 | 63.9 | 59.1 | 52.8 | 59.2 | 15.0 | 10.6 | 19.8 | 42.4 | 65.9 | 59.1 | 46.1 | 31.4 | 19.3 | 50.7 | 63.6 | 23.8 |
| DLv3+ (X71) | 78.6 | 64.1 | 60.9 | 52.0 | 60.4 | 14.9 | 10.8 | 19.4 | 41.2 | 68.0 | 58.7 | 47.1 | 40.2 | 18.8 | 50.4 | 64.1 | 20.2 |
| ICNet | 65.9 | 45.8 | 44.6 | 47.4 | 44.7 | 8.4 | 8.4 | 10.6 | 27.9 | 41.0 | 33.1 | 27.5 | 34.0 | 6.3 | 30.5 | 27.3 | 11.0 |
| FCN8s | 66.7 | 42.7 | 31.1 | 37.0 | 34.1 | 6.7 | 5.7 | 7.8 | 24.9 | 53.3 | 39.0 | 36.0 | 21.2 | 11.3 | 31.6 | 37.6 | 19.7 |
| DilatedNet | 68.6 | 44.4 | 36.3 | 32.5 | 38.4 | 15.6 | 14.0 | 18.4 | 32.7 | 52.7 | 32.6 | 38.1 | 29.1 | 12.5 | 32.3 | 34.7 | 19.2 |
| ResNet-38 | 77.5 | 54.6 | 45.1 | 43.3 | 47.2 | 13.7 | 16.0 | 18.2 | 38.3 | 60.0 | 50.6 | 46.9 | 14.7 | 13.5 | 45.9 | 52.9 | 22.2 |
| PSPNet | 78.8 | 59.8 | 53.2 | 44.4 | 53.9 | 11.0 | 15.4 | 15.4 | 34.2 | 60.4 | 51.8 | 30.6 | 21.4 | 8.4 | 42.7 | 34.4 | 16.2 |
| GSCNN | 80.9 | 58.9 | 58.4 | 41.9 | 60.1 | 5.5 | 2.6 | 6.8 | 24.7 | 75.9 | 61.9 | 70.7 | 12.0 | 12.4 | 47.3 | 67.9 | 32.6 |
| SegFormer-B5 | 82.4 | 69.1 | 68.6 | 64.1 | 69.8 | 57.8 | 63.4 | 52.3 | 72.8 | 81.0 | 77.7 | 80.1 | 58.8 | 40.7 | 68.4 | 78.5 | 49.9 |

5 Conclusion

In this paper, we present SegFormer, a simple, clean yet powerful semantic segmentation method which contains a positional-encoding-free, hierarchical Transformer encoder and a lightweight All-MLP decoder. It avoids common complex designs in previous methods, leading to both high efficiency and performance. SegFormer not only achieves new state of the art results on common datasets, but also shows strong zero-shot robustness. We hope our method can serve as a solid baseline for semantic segmentation and motivate further research. One limitation is that although our smallest 3.7M parameters model is smaller than the known CNN’s model, it is unclear whether it can work well in a chip of edge device with only 100k memory. We leave it for future work.

Acknowledgement

We thank Ding Liang, Zhe Chen and Yaojun Liu for insightful discussion without which this paper would not be possible.

A Details of MiT Series

In this section, we list some important hyper-parameters of our Mix Transformer (MiT) encoder. By changing these parameters, we can easily scale up our encoder from B0 to B5.

In summary, the hyper-parameters of our MiT are listed as follows:

- K_i : the patch size of the overlapping patch embedding in Stage i ;

- S_i : the stride of the overlapping patch embedding in Stage i ;
- P_i : the padding size of the overlapping patch embedding in Stage i ;
- C_i : the channel number of the output of Stage i ;
- L_i : the number of encoder layers in Stage i ;
- R_i : the reduction ratio of the Efficient Self-Attention in Stage i ;
- N_i : the head number of the Efficient Self-Attention in Stage i ;
- E_i : the expansion ratio of the feed-forward layer [78] in Stage i ;

Table 6 shows the detailed information of our MiT series. To facilitate efficient discussion, we assign the code name B0 to B5 for MiT encoder, where B0 is the smallest model designed for real-time, while B5 is the largest model designed for high performance.

B More Qualitative Results on Mask Predictions

In Figure 5, we present more qualitative results on Cityscapes, ADE20K and COCO-Stuff, compared with SETR and DeepLabV3+.

Compared to SETR, our SegFormer predicts masks with significantly finer details near object boundaries because our Transformer encoder can capture much higher resolution features than SETR, which preserves more detailed texture information. Compared to DeepLabV3+, SegFormer reduces long-range errors benefit from the larger effective receptive field of Transformer encoder than ConvNet.

C More Visualization on Effective Receptive Field

In Figure 6, we select some representative images and effective receptive field (ERF) of DeepLabV3+ and SegFormer. Beyond larger ERF, the ERF of SegFormer is more sensitive to the context of the image. We see SegFormer’s ERF learned the pattern of roads, cars, and buildings, while DeepLabV3+’s ERF shows a relatively fixed pattern. The results also indicate that our Transformer encoder has a stronger feature extraction ability than ConvNets.

D More Comparison of DeeplabV3+ and SegFormer on Cityscapes-C

In this section, we detailed show the zero-shot robustness compared with SegFormer and DeepLabV3+. Following [77], we test 3 severities for 4 kinds of “Noise” and 5 severities for the rest 12 kinds of corruptions and perturbations.

As shown in Figure 7, with severity increase, DeepLabV3+ shows a considerable performance degradation. In contrast, the performance of SegFormer is relatively stable. Moreover, SegFormer has significant advantages over DeepLabV3+ on all corruptions/perturbations and all severities, demonstrating excellent zero-shot robustness.

| | Output Size | Layer Name | Mix Transformer | | | | | | | |
|---------------------|------------------------------------|-----------------------------|-----------------------------|-----------|-----------|------------|-------------|------------|--|--|
| | | | B0 | B1 | B2 | B3 | B4 | B5 | | |
| Stage 1 | $\frac{H}{4} \times \frac{W}{4}$ | Overlapping Patch Embedding | $K_1 = 7; S_1 = 4; P_1 = 3$ | | | | | | | |
| | | | $C_1 = 32$ | | | | $C_1 = 64$ | | | |
| Stage 2 | $\frac{H}{8} \times \frac{W}{8}$ | Overlapping Patch Embedding | $K_2 = 3; S_2 = 2; P_2 = 1$ | | | | | | | |
| | | | $C_2 = 64$ | | | | $C_2 = 128$ | | | |
| Stage 3 | $\frac{H}{16} \times \frac{W}{16}$ | Overlapping Patch Embedding | $K_3 = 3; S_3 = 2; P_3 = 1$ | | | | | | | |
| | | | $C_3 = 160$ | | | | $C_3 = 320$ | | | |
| Stage 4 | $\frac{H}{32} \times \frac{W}{32}$ | Overlapping Patch Embedding | $K_4 = 3; S_4 = 2; P_4 = 1$ | | | | | | | |
| | | | $C_4 = 256$ | | | | $C_4 = 512$ | | | |
| Transformer Encoder | | | $R_1 = 8$ | $R_1 = 8$ | $R_1 = 8$ | $R_1 = 8$ | $R_1 = 8$ | $R_1 = 8$ | | |
| | | | $N_1 = 1$ | $N_1 = 1$ | $N_1 = 1$ | $N_1 = 1$ | $N_1 = 1$ | $N_1 = 1$ | | |
| | | | $E_1 = 8$ | $E_1 = 8$ | $E_1 = 8$ | $E_1 = 8$ | $E_1 = 8$ | $E_1 = 4$ | | |
| | | | $L_1 = 2$ | $L_1 = 2$ | $L_1 = 3$ | $L_1 = 3$ | $L_1 = 3$ | $L_1 = 3$ | | |
| Transformer Encoder | | | $R_2 = 4$ | $R_2 = 4$ | $R_2 = 4$ | $R_2 = 4$ | $R_2 = 4$ | $R_2 = 4$ | | |
| | | | $N_2 = 2$ | $N_2 = 2$ | $N_2 = 2$ | $N_2 = 2$ | $N_2 = 2$ | $N_2 = 2$ | | |
| | | | $E_2 = 8$ | $E_2 = 8$ | $E_2 = 8$ | $E_2 = 8$ | $E_2 = 8$ | $E_2 = 4$ | | |
| | | | $L_2 = 2$ | $L_2 = 2$ | $L_2 = 3$ | $L_2 = 3$ | $L_2 = 8$ | $L_2 = 6$ | | |
| Transformer Encoder | | | $R_3 = 2$ | $R_3 = 2$ | $R_3 = 2$ | $R_3 = 2$ | $R_3 = 2$ | $R_3 = 2$ | | |
| | | | $N_3 = 5$ | $N_3 = 5$ | $N_3 = 5$ | $N_3 = 5$ | $N_3 = 5$ | $N_3 = 5$ | | |
| | | | $E_3 = 4$ | $E_3 = 4$ | $E_3 = 4$ | $E_3 = 4$ | $E_3 = 4$ | $E_3 = 4$ | | |
| | | | $L_3 = 2$ | $L_3 = 2$ | $L_3 = 6$ | $L_3 = 18$ | $L_3 = 27$ | $L_3 = 40$ | | |
| Transformer Encoder | | | $R_4 = 1$ | $R_4 = 1$ | $R_4 = 1$ | $R_4 = 1$ | $R_4 = 1$ | $R_4 = 1$ | | |
| | | | $N_4 = 8$ | $N_4 = 8$ | $N_4 = 8$ | $N_4 = 8$ | $N_4 = 8$ | $N_4 = 8$ | | |
| | | | $E_4 = 4$ | $E_4 = 4$ | $E_4 = 4$ | $E_4 = 4$ | $E_4 = 4$ | $E_4 = 4$ | | |
| | | | $L_4 = 2$ | $L_4 = 2$ | $L_4 = 3$ | $L_4 = 3$ | $L_4 = 3$ | $L_4 = 3$ | | |

Table 6: **Detailed settings of MiT series.** Our design follows the principles of ResNet [12]. (1) the channel dimension increase while the spatial resolution shrink with the layer goes deeper. (2) Stage 3 is assigned to most of the computation cost.

| Method | GFLOPs | Params (M) | Top 1 |
|--------|--------|------------|-------|
| MiT-B0 | 0.6 | 3.7 | 70.5 |
| MiT-B1 | 2.1 | 14.0 | 78.7 |
| MiT-B2 | 4.0 | 25.4 | 81.6 |
| MiT-B3 | 6.9 | 45.2 | 83.1 |
| MiT-B4 | 10.1 | 62.6 | 83.6 |
| MiT-B5 | 11.8 | 82.0 | 83.8 |

Table 7: Mix Transformer Encoder

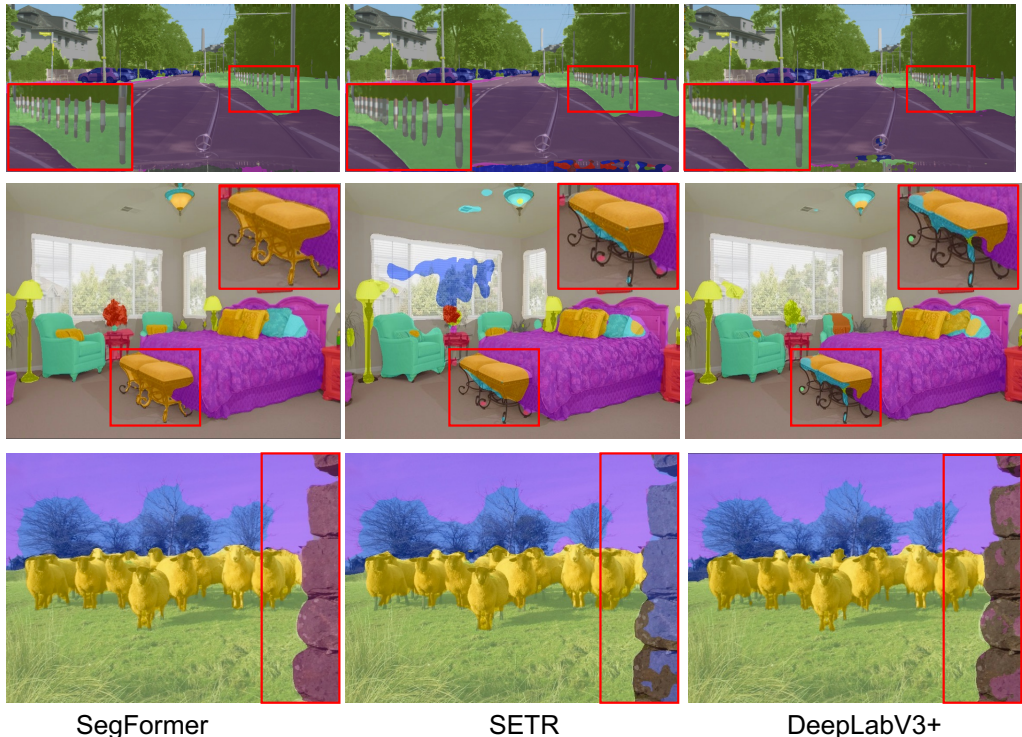


Figure 5: **Qualitative results on Cityscapes, ADE20K and COCO-Stuff.** First row: Cityscapes. Second row: ADE20K. Third row: COCO-Stuff. Zoom in for best view.

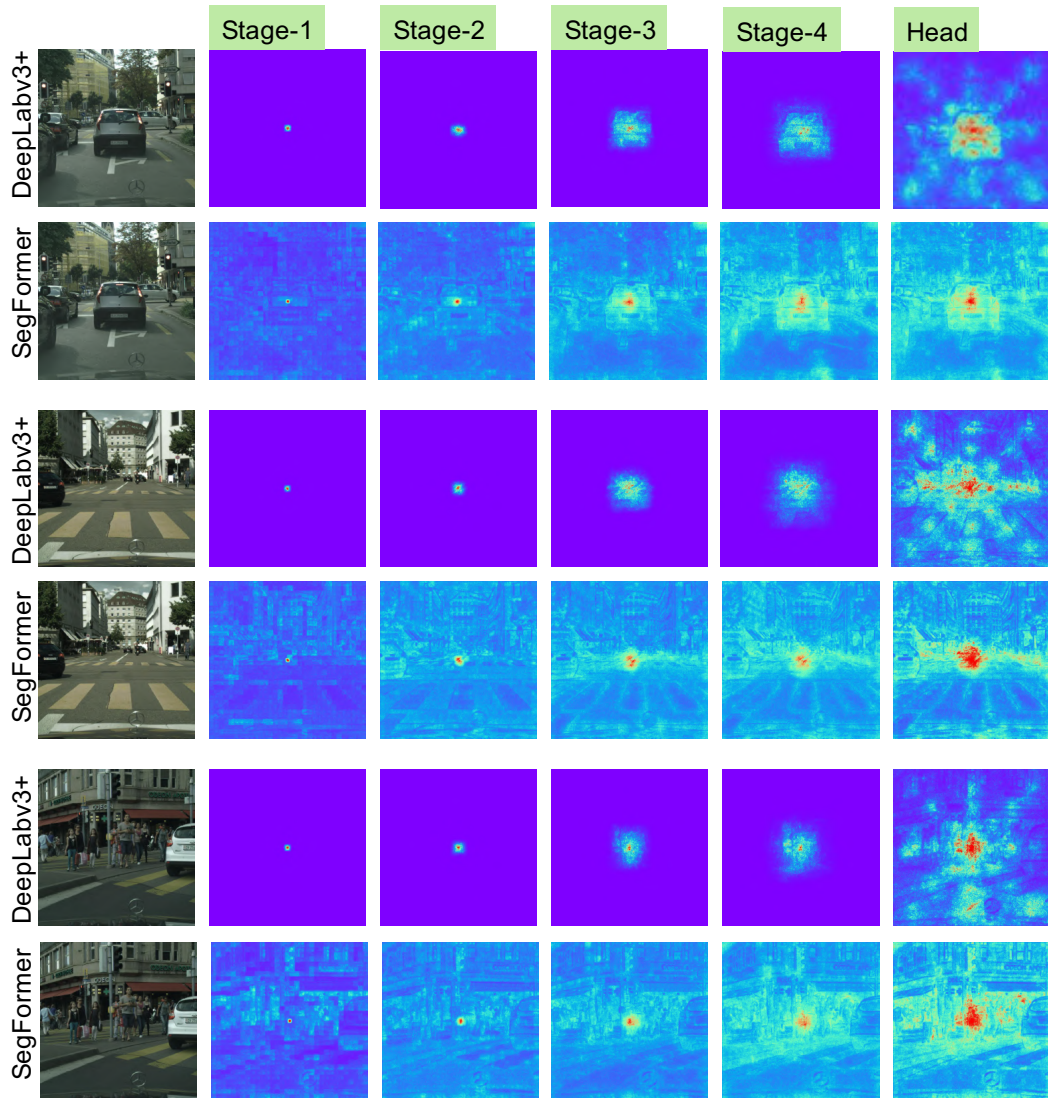


Figure 6: **Effective Receptive Field on Cityscapes.** ERFs of the four stages and the decoder heads of both architectures are visualized.

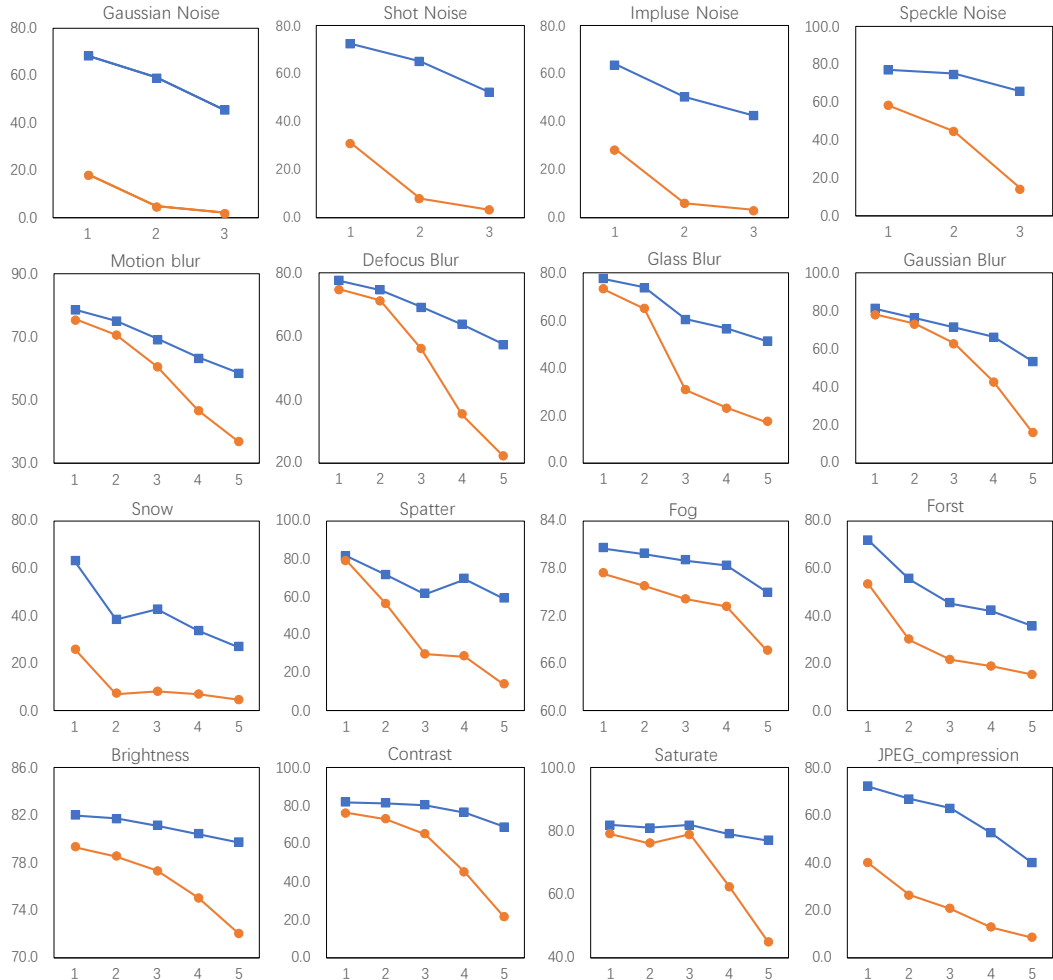


Figure 7: Comparison of zero shot robustness on Cityscapes-C between SegFormer and DeepLabV3+. Blue line is SegFormer and orange line is DeepLabV3+. X-Axis means corrupt severity and Y-Axis is mIoU. Following [77], we test 3 severities for “Noise” and 5 severities for the rest.

References

- [1] Jonathan Long, Evan Shelhamer, and Trevor Darrell. Fully convolutional networks for semantic segmentation. In *CVPR*, 2015. 1, 2, 7
- [2] Liang-Chieh Chen, George Papandreou, Iasonas Kokkinos, Kevin Murphy, and Alan L Yuille. Semantic image segmentation with deep convolutional nets and fully connected CRFs. In *ICLR*, 2015. 1, 2
- [3] Hang Zhang, Chongruo Wu, Zhongyue Zhang, Yi Zhu, Haibin Lin, Zhi Zhang, Yue Sun, Tong He, Jonas Mueller, R Manmatha, et al. ResNest: Split-attention networks. *arXiv*, 2020. 1
- [4] Liang-Chieh Chen, George Papandreou, Iasonas Kokkinos, Kevin Murphy, and Alan L Yuille. Deeplab: Semantic image segmentation with deep convolutional nets, atrous convolution, and fully connected CRFs. *TPAMI*, 2017. 2
- [5] Fisher Yu and Vladlen Koltun. Multi-scale context aggregation by dilated convolutions. In *ICLR*, 2016. 2, 5
- [6] Alexey Dosovitskiy, Lucas Beyer, Alexander Kolesnikov, Dirk Weissenborn, Xiaohua Zhai, Thomas Unterthiner, Mostafa Dehghani, Matthias Minderer, Georg Heigold, Sylvain Gelly, et al. An image is worth 16x16 words: Transformers for image recognition at scale. *arXiv*, 2020. 2, 3
- [7] Sixiao Zheng, Jiachen Lu, Hengshuang Zhao, Xiatian Zhu, Zekun Luo, Yabiao Wang, Yanwei Fu, Jianfeng Feng, Tao Xiang, Philip HS Torr, et al. Rethinking semantic segmentation from a sequence-to-sequence perspective with transformers. *CVPR*, 2021. 2, 3, 5, 7, 8
- [8] Wenhai Wang, Enze Xie, Xiang Li, Deng-Ping Fan, Kaitao Song, Ding Liang, Tong Lu, Ping Luo, and Ling Shao. Pyramid vision transformer: A versatile backbone for dense prediction without convolutions. *arXiv*, 2021. 2, 3, 4
- [9] Ze Liu, Yutong Lin, Yue Cao, Han Hu, Yixuan Wei, Zheng Zhang, Stephen Lin, and Baining Guo. Swin transformer: Hierarchical vision transformer using shifted windows. *arXiv*, 2021. 2, 3, 6
- [10] Xiangxiang Chu, Zhi Tian, Yuqing Wang, Bo Zhang, Haibing Ren, Xiaolin Wei, Huaxia Xia, and Chunhua Shen. Twins: Revisiting spatial attention design in vision transformers. *arXiv*, 2021. 2, 3
- [11] Hengshuang Zhao, Xiaojuan Qi, Xiaoyong Shen, Jianping Shi, and Jiaya Jia. Icnet for real-time semantic segmentation on high-resolution images. In *ECCV*, 2018. 2, 7
- [12] Kaiming He, Xiangyu Zhang, Shaoqing Ren, and Jian Sun. Deep residual learning for image recognition. In *CVPR*, 2016. 2, 11
- [13] Alex Krizhevsky, Ilya Sutskever, and Geoffrey E Hinton. Imagenet classification with deep convolutional neural networks. *NeurIPS*, 2012.
- [14] Karen Simonyan and Andrew Zisserman. Very deep convolutional networks for large-scale image recognition. *arXiv*, 2014.
- [15] Xiang Li, Wenhai Wang, Xiaolin Hu, and Jian Yang. Selective kernel networks. In *CVPR*, 2019.
- [16] Wenhai Wang, Xiang Li, Tong Lu, and Jian Yang. Mixed link networks. In *IJCAI*, 2018. 2
- [17] Hengshuang Zhao, Jianping Shi, Xiaojuan Qi, Xiaogang Wang, and Jiaya Jia. Pyramid scene parsing network. In *CVPR*, 2017. 2, 7, 8
- [18] Maoke Yang, Kun Yu, Chi Zhang, Zhiwei Li, and Kuiyuan Yang. Denseaspp for semantic segmentation in street scenes. In *CVPR*, 2018. 5
- [19] Chao Peng, Xiangyu Zhang, Gang Yu, Guiming Luo, and Jian Sun. Large kernel matters—improve semantic segmentation by global convolutional network. In *CVPR*, 2017. 2, 5
- [20] Liang-Chieh Chen, Yukun Zhu, George Papandreou, Florian Schroff, and Hartwig Adam. Encoder-decoder with atrous separable convolution for semantic image segmentation. In *ECCV*, 2018. 2, 5, 7, 8
- [21] Yuhui Yuan and Jingdong Wang. Ocnet: Object context network for scene parsing. *arXiv*, 2018. 2, 8
- [22] Changqian Yu, Jingbo Wang, Changxin Gao, Gang Yu, Chunhua Shen, and Nong Sang. Context prior for scene segmentation. In *CVPR*, 2020.

- [23] Yuhui Yuan, Xilin Chen, and Jingdong Wang. Object-contextual representations for semantic segmentation. *arXiv*, 2019. 7, 8
- [24] Hang Zhang, Kristin Dana, Jianping Shi, Zhongyue Zhang, Xiaogang Wang, Ambrish Tyagi, and Amit Agrawal. Context encoding for semantic segmentation. In *CVPR*, 2018. 7
- [25] Yizhou Zhou, Xiaoyan Sun, Zheng-Jun Zha, and Wenjun Zeng. Context-reinforced semantic segmentation. In *CVPR*, 2019.
- [26] Guosheng Lin, Anton Milan, Chunhua Shen, and Ian Reid. Refinenet: Multi-path refinement networks for high-resolution semantic segmentation. In *CVPR*, 2017.
- [27] Rudra PK Poudel, Ujwal Bonde, Stephan Liwicki, and Christopher Zach. Contextnet: Exploring context and detail for semantic segmentation in real-time. *arXiv*, 2018.
- [28] Tianyi Wu, Sheng Tang, Rui Zhang, and Yongdong Zhang. Cgnet: A light-weight context guided network for semantic segmentation. *arXiv*, 2018.
- [29] Junjun He, Zhongying Deng, Lei Zhou, Yali Wang, and Yu Qiao. Adaptive pyramid context network for semantic segmentation. In *CVPR*, 2019. 3
- [30] Henghui Ding, Xudong Jiang, Ai Qun Liu, Nadia Magnenat Thalmann, and Gang Wang. Boundary-aware feature propagation for scene segmentation. In *ICCV*, 2019. 3
- [31] Gedas Bertasius, Jianbo Shi, and Lorenzo Torresani. Semantic segmentation with boundary neural fields. In *CVPR*, 2016.
- [32] Xiangtai Li, Xia Li, Li Zhang, Guangliang Cheng, Jianping Shi, Zhouchen Lin, Shaohua Tan, and Yunhai Tong. Improving semantic segmentation via decoupled body and edge supervision. *arxiv*, 2020.
- [33] Yuhui Yuan, Jingyi Xie, Xilin Chen, and Jingdong Wang. Segfix: Model-agnostic boundary refinement for segmentation. In *ECCV*, 2020.
- [34] Mingmin Zhen, Jinglu Wang, Lei Zhou, Shiwei Li, Tianwei Shen, Jiaxiang Shang, Tian Fang, and Long Quan. Joint semantic segmentation and boundary detection using iterative pyramid contexts. In *CVPR*, 2020.
- [35] Towaki Takikawa, David Acuna, Varun Jampani, and Sanja Fidler. Gated-scnn: Gated shape cnns for semantic segmentation. In *ICCV*, 2019. 7
- [36] Changqian Yu, Jingbo Wang, Chao Peng, Changxin Gao, Gang Yu, and Nong Sang. Learning a discriminative feature network for semantic segmentation. In *CVPR*, 2018.
- [37] Liang-Chieh Chen, Jonathan T Barron, George Papandreou, Kevin Murphy, and Alan L Yuille. Semantic image segmentation with task-specific edge detection using cnns and a discriminatively trained domain transform. In *CVPR*, 2016. 3
- [38] Jun Fu, Jing Liu, Haijie Tian, Yong Li, Yongjun Bao, Zhiwei Fang, and Hanqing Lu. Dual attention network for scene segmentation. In *CVPR*, 2019. 3
- [39] Xiaolong Wang, Ross Girshick, Abhinav Gupta, and Kaiming He. Non-local neural networks. In *CVPR*, 2018.
- [40] Zilong Zhong, Zhong Qiu Lin, Rene Bidart, Xiaodan Hu, Ibrahim Ben Daya, Zhifeng Li, Wei-Shi Zheng, Jonathan Li, and Alexander Wong. Squeeze-and-attention networks for semantic segmentation. In *CVPR*, 2020.
- [41] Zilong Huang, Xinggang Wang, Lichao Huang, Chang Huang, Yunchao Wei, and Wenyu Liu. Ccnet: Criss-cross attention for semantic segmentation. In *ICCV*, 2019. 7, 8
- [42] Hanchao Li, Pengfei Xiong, Jie An, and Lingxue Wang. Pyramid attention network for semantic segmentation. *arXiv*, 2018.
- [43] Hengshuang Zhao, Yi Zhang, Shu Liu, Jianping Shi, Chen Change Loy, Dahua Lin, and Jiaya Jia. Psanet: Point-wise spatial attention network for scene parsing. In *ECCV*, 2018. 8
- [44] Xia Li, Zhisheng Zhong, Jianlong Wu, Yibo Yang, Zhouchen Lin, and Hong Liu. Expectation-maximization attention networks for semantic segmentation. In *ICCV*, 2019.

- [45] Yue Cao, Jiarui Xu, Stephen Lin, Fangyun Wei, and Han Hu. Gcnet: Non-local networks meet squeeze-excitation networks and beyond. In *ICCVW*, 2019.
- [46] Enze Xie, Wenjia Wang, Wenhui Wang, Peize Sun, Hang Xu, Ding Liang, and Ping Luo. Segmenting transparent object in the wild with transformer. *IJCAI*, 2021. 3
- [47] Albert Shaw, Daniel Hunter, Forrest Landola, and Sammy Sidhu. Squeezeenas: Fast neural architecture search for faster semantic segmentation. In *ICCVW*, 2019. 3
- [48] Wuyang Chen, Xinyu Gong, Xianming Liu, Qian Zhang, Yuan Li, and Zhangyang Wang. Fasterseg: Searching for faster real-time semantic segmentation. *arXiv*, 2019.
- [49] Yanwei Li, Lin Song, Yukang Chen, Zeming Li, Xiangyu Zhang, Xingang Wang, and Jian Sun. Learning dynamic routing for semantic segmentation. In *CVPR*, 2020.
- [50] Chenxi Liu, Liang-Chieh Chen, Florian Schroff, Hartwig Adam, Wei Hua, Alan L Yuille, and Li Fei-Fei. Auto-deeplab: Hierarchical neural architecture search for semantic image segmentation. In *CVPR*, 2019. 7
- [51] Vladimir Nekrasov, Hao Chen, Chunhua Shen, and Ian Reid. Fast neural architecture search of compact semantic segmentation models via auxiliary cells. In *CVPR*, 2019. 3
- [52] Nicolas Carion, Francisco Massa, Gabriel Synnaeve, Nicolas Usunier, Alexander Kirillov, and Sergey Zagoruyko. End-to-End object detection with transformers. In *ECCV*, 2020. 3
- [53] Li Yuan, Yunpeng Chen, Tao Wang, Weihao Yu, Yujun Shi, Zihang Jiang, Francis EH Tay, Jiashi Feng, and Shuicheng Yan. Tokens-to-token vit: Training vision transformers from scratch on imagenet. *arXiv*, 2021. 3
- [54] Xiangxiang Chu, Zhi Tian, Bo Zhang, Xinlong Wang, Xiaolin Wei, Huaxia Xia, and Chunhua Shen. Conditional positional encodings for vision transformers. *arXiv*, 2021. 3, 4
- [55] Kai Han, An Xiao, Enhua Wu, Jianyuan Guo, Chunjing Xu, and Yunhe Wang. Transformer in transformer. *arXiv*, 2021. 3
- [56] Chun-Fu Chen, Quanfu Fan, and Rameswar Panda. Crossvit: Cross-attention multi-scale vision transformer for image classification. *arXiv*, 2021. 3
- [57] Yawei Li, Kai Zhang, Jiezhang Cao, Radu Timofte, and Luc Van Gool. Localvit: Bringing locality to vision transformers. *arXiv*, 2021. 3
- [58] Haiping Wu, Bin Xiao, Noel Codella, Mengchen Liu, Xiyang Dai, Lu Yuan, and Lei Zhang. Cvt: Introducing convolutions to vision transformers. *arXiv*, 2021. 3
- [59] Weijian Xu, Yifan Xu, Tyler Chang, and Zhuowen Tu. Co-scale conv-attentional image transformers. *arXiv*, 2021. 3
- [60] Ben Graham, Alaaeldin El-Nouby, Hugo Touvron, Pierre Stock, Armand Joulin, Hervé Jégou, and Matthijs Douze. Levit: a vision transformer in convnet’s clothing for faster inference. *arXiv*, 2021. 3
- [61] Peize Sun, Yi Jiang, Rufeng Zhang, Enze Xie, Jinkun Cao, Xinting Hu, Tao Kong, Zehuan Yuan, Changhu Wang, and Ping Luo. Trantrack: Multiple-object tracking with transformer. *arXiv*, 2020. 3
- [62] Tim Meinhardt, Alexander Kirillov, Laura Leal-Taixe, and Christoph Feichtenhofer. Trackformer: Multi-object tracking with transformers. *arXiv*, 2021. 3
- [63] Hanting Chen, Yunhe Wang, Tianyu Guo, Chang Xu, Yiping Deng, Zhenhua Liu, Siwei Ma, Chunjing Xu, Chao Xu, and Wen Gao. Pre-trained image processing transformer. *arXiv*, 2020. 3
- [64] Shuting He, Hao Luo, Pichao Wang, Fan Wang, Hao Li, and Wei Jiang. Transreid: Transformer-based object re-identification. *arXiv*, 2021. 3
- [65] Manoj Kumar, Dirk Weissenborn, and Nal Kalchbrenner. Colorization transformer. *arXiv*, 2021. 3
- [66] Alaaeldin El-Nouby, Natalia Neverova, Ivan Laptev, and Hervé Jégou. Training vision transformers for image retrieval. *arXiv*, 2021. 3
- [67] Alec Radford, Jong Wook Kim, Chris Hallacy, Aditya Ramesh, Gabriel Goh, Sandhini Agarwal, Girish Sastry, Amanda Askell, Pamela Mishkin, Jack Clark, et al. Learning transferable visual models from natural language supervision. *arXiv*, 2021. 3

- [68] Ronghang Hu and Amanpreet Singh. Transformer is all you need: Multimodal multitask learning with a unified transformer. *arXiv*, 2021. 3
- [69] Md Amirul Islam, Sen Jia, and Neil DB Bruce. How much position information do convolutional neural networks encode? *arXiv*, 2020. 4
- [70] Wenjie Luo, Yujia Li, Raquel Urtasun, and Richard Zemel. Understanding the effective receptive field in deep convolutional neural networks. *arXiv*, 2017. 5
- [71] Marius Cordts, Mohamed Omran, Sebastian Ramos, Timo Rehfeld, Markus Enzweiler, Rodrigo Benenson, Uwe Franke, Stefan Roth, and Bernt Schiele. The cityscapes dataset for semantic urban scene understanding. In *CVPR*, 2016. 6, 8
- [72] Bolei Zhou, Hang Zhao, Xavier Puig, Sanja Fidler, Adela Barriuso, and Antonio Torralba. Scene parsing through ade20k dataset. In *CVPR*, 2017. 6, 8
- [73] Holger Caesar, Jasper Uijlings, and Vittorio Ferrari. Coco-stuff: Thing and stuff classes in context. In *CVPR*, 2018. 6, 8
- [74] Huiyu Wang, Yukun Zhu, Bradley Green, Hartwig Adam, Alan L. Yuille, and Liang-Chieh Chen. Axial-deeplab: Stand-alone axial-attention for panoptic segmentation. In *ECCV*, 2020. 7, 8
- [75] Yanwei Li, Lin Song, Yukang Chen, Zeming Li, Xiangyu Zhang, Xingang Wang, and Jian Sun. Learning dynamic routing for semantic segmentation. In *CVPR*, 2020. 7
- [76] Gerhard Neuhold, Tobias Ollmann, Samuel Rota Bulò, and Peter Kuntschieder. The mapillary vistas dataset for semantic understanding of street scenes. In *ICCV*, 2017. 8
- [77] Christoph Kamann and Carsten Rother. Benchmarking the robustness of semantic segmentation models. In *CVPR*, 2020. 8, 9, 10, 14
- [78] Ashish Vaswani, Noam Shazeer, Niki Parmar, Jakob Uszkoreit, Llion Jones, Aidan N Gomez, Łukasz Kaiser, and Illia Polosukhin. Attention is all you need. In *NeurIPS*, 2017. 10